Check for updates

# Spatially separated bimetallic cocatalysts on hollow-structured TiO$_2$ for photocatalytic hydrogen generation†

Ping She, [ID] [a] Jun-sheng Qin, [ID] [ab] Heng Rao, [ID] [ab] Buyuan Guan [ab] and Jihong Yu [ID] *[ab]

Efficient charge separation and light harvesting of photocatalysts (*e.g.*, TiO$_2$) are the key issues to be considered in the design of solar-energy conversion systems. In particular, the charge separation of noble metal-decorated TiO$_2$ materials could be greatly improved *via* decreasing the size of noble metal particles (NPs). Furthermore, designing specific morphologies such as hollow structures can improve light harvesting ability. Herein, a hybrid hollow TiO$_2$ with spatially separated bimetals (Pd@TiO$_2$@Au) was prepared, which demonstrated enhanced charge separation. By choosing zeolite as the sacrificial substrate, ultrasmall Pd NPs and Au NPs were decorated in the inner and outer shells of hollow TiO$_2$, respectively. The separated bimetals could pull the photoexcited electrons away from the surface of TiO$_2$ for more efficient charge separation. The as-prepared Pd@TiO$_2$@Au catalyst exhibited a superior photocatalytic H$_2$ evolution rate up to 272.3 μmol h$^{-1}$, which was higher than most of the TiO$_2$-based photocatalysts.

## Introduction

Nowadays, the problem of energy shortage and environmental pollution is becoming more and more serious in the world.[1–5] Hydrogen (H$_2$) as a kind of clean fuel has drawn intensive attention for its superior energy density and environmental friendliness.[1–3] Converting solar energy into H$_2$ by photocatalytic water splitting is one of the most efficient ways for H$_2$ production. A large number of semiconductor photocatalysts including titanium dioxide (TiO$_2$), CdS, Ta$_3$N$_5$, ZnO and g-C$_3$N$_4$ have been widely used for photocatalytic H$_2$ generation.[6,7] Among them, TiO$_2$ has been considered as one of the most promising photocatalysts owing to its low price, high safety and superior chemical stability.[8–11] However, the fast recombination of the photogenerated electron–hole pairs strongly hinders the photocatalytic hydrogen production. Recently, noble metal nanoparticles (NPs) (*e.g.*, Au, Pt, and Ag NPs) were decorated on photocatalysts to enhance the catalytic properties.[12–15] In particular, the bimetal decorated TiO$_2$ (such as Pd–Au, Pt–Cu, and Au–Pt) can exhibit further improved photocatalytic efficiency compared to the

monometal decorated ones.[16–20] Among them, most of the bimetals were randomly decorated outside the TiO$_2$ with the inner interface not being used. Thus, the spatially separated bimetals on the inner and outer surfaces of TiO$_2$ are expected to be able to enhance the photocatalytic properties by fully utilizing the photo-induced charges on the interface of excited TiO$_2$.

On the other hand, recent investigations showed that the size of noble metal NPs has a great influence on the photocatalytic properties of the nanohybrids.[6,21] It has been demonstrated that the smaller noble metal NPs can induce a lower Fermi level, which can cause improved charge transfer and an elevated separation rate of electron–hole pairs.[21] Unfortunately, it is hard to obtain ultrasmall noble metal clusters since they are prone to aggregation. Nowadays, zeolites have been widely used for the confinement synthesis of ultrasmall metal NPs and even sub-nanometric metallic clusters, in which the nanospace of zeolites can restrict the growth of the metals.[22–24] Also, the ordered microporous structures of zeolites can eliminate the aggregation of metal species and thus improve the catalytic properties and stability.[25]

Furthermore, it has been demonstrated that the nanostructures of the hybrids of noble metal–TiO$_2$ play an important role in improving the photocatalytic properties.[11,26–30] Notably, the nano hybrids with a yolk–shelled hollow morphology can induce higher photocatalytic properties.[30] On the one hand, the hollow structure can enhance light utilization efficiency by realizing repeated light reflection and refraction; on the other hand, the hollow structure can increase the surface-to-volume ratio,

[a] State Key Laboratory of Inorganic Synthesis and Preparative Chemistry, College of Chemistry, Jilin University, 2699 Qianjin Street, Changchun 130012, P. R. China. E-mail: jihong@jlu.edu.cn

[b] International Center of Future Science, Jilin University, 2699 Qianjin Street, Changchun 130012, P. R. China

† Electronic supplementary information (ESI) available: Additional characterization results including SEM images, TEM images, EDS mapping images, XRD patterns, and time courses of photocatalytic H$_2$ evolution. See DOI: 10.1039/d0qm00042f

which can provide more active reaction sites and enhance mass transfer.

Herein, we designed a hollow-structured $TiO_2$ with spatially separated bimetallic NPs decorated in the core and outer shells, respectively. In detail, the hollow $TiO_2$ sphere was obtained by choosing silicalite-1 (MFI) zeolite with embedded ultrasmall Pd NPs as a supporting substrate followed by etching of the zeolite. The $TiO_2$ exhibited a hollow structure and the ultrasmall Pd NPs were decorated inside the hollow $TiO_2$ sphere. Then, Au NPs working as the cocatalyst were decorated on the outer surfaces of the $TiO_2$ shell. The obtained sandwich-like hollow-structured $Pd@TiO_2@Au$ with spatially separated cocatalysts can significantly enhance the photocatalytic properties of $TiO_2$ by combining the surface plasmon resonance (SPR) effect of Au NPs and the smaller size effect of Pd NPs. Specifically, $Pd@TiO_2@Au$ exhibited a superior photocatalytic $H_2$ evolution rate up to 272.3 μmol $h^{-1}$. Such performance is far superior to most of the $TiO_2$-based photocatalysts for water-splitting.

## Experimental

### Materials

Chloroauric acid tetrahydrate ($HAuCl_4 \cdot 4H_2O$, A.R., Shanghai Chemical Factory), tetraethylorthosilicate (TEOS) (Sinopharm Chemical Reagent Co., Ltd), tetrabutyl orthotitanate (TBOT) (98%, Macklin), tetrapropylammonium hydroxide (TPAOH) (25 wt%, Tianjin Guangfu Fine Chemical Research Institute), ethanol (99%, Tianjin Guangfu Fine Chemical Research Institute), palladium chloride ($PdCl_2$, Pd 59%, Aladdin), ethylenediamine ($NH_2CH_2CH_2NH_2$, Tianjin Fuchen Chemical Reagents Factory), ammonia ($NH_3 \cdot H_2O$, Tianjin Yongsheng Fine Chemical Co., Ltd), sodium hydroxide (NaOH, A.R., Tianjin Yongsheng Fine Chemical Co., Ltd), and deionized water (resistance $> 18$ MΩ $cm^{-1}$).

### Preparation of silicalite-1 (S1) zeolite

S1 was prepared by using the hydrothermal method at 170 °C for 4 days, the molar composition of which is $1.0SiO_2:0.4$ $TPAOH:35H_2O$. Specifically, 13 g of TPAOH was mixed with deionized water followed by stirring for 10 min, then 8.32 g of TEOS was added to the above solution. After being stirred for 6 h, the mixture was transferred to a Teflon-lined stainless-steel autoclave and heated at 170 °C for 4 days under static conditions. After washing with deionized water and ethanol three times, the product was then dried at 60 °C. Finally, conventional S1 was obtained by calcinating the above product at 550 °C in air for 8 h.

### Synthesis of Pd@silicalite-1 (Pd@S1)

Pd@S1 was synthesized using the same method for the preparation of S1 except for the addition of $[Pd(NH_2CH_2CH_2NH_2)_2]Cl_2$ after the hydrolysis of TEOS.[27] After calcination, the product was subsequently reduced with $H_2$ at 400 °C for 2 h. In this way, Pd@S1 was obtained.

### Preparation of hollow Pd@TiO₂, hollow TiO₂ and TiO₂ NPs

Typically, 150 mg of the above-synthesized zeolite or Pd@S1 was dispersed in 200 mL of absolute ethanol. After adding 0.9 mL of ammonia solution (28 wt%) into the system followed by ultrasonication for half an hour, TBOT (2.0 mL) was added into the solution drop by drop. Then, the mixture was stirred at 45 °C for 24 hours. After washing with deionized water and ethanol several times and calcination at 450 °C for 2 h, $Pd@S1@TiO_2$ NPs were obtained. In order to get hollow structured $Pd@TiO_2$, 50 mg of $Pd@S1@TiO_2$ NPs was treated with 30 mL of NaOH solution (3 M) under stirring for 12 h. After centrifugation and washing with water and ethanol 3 times, hollow $Pd@TiO_2$ was obtained. When it comes to the synthesis of hollow $TiO_2$ NPs, S1 was used to replace Pd@S1. The conventional $TiO_2$ NPs were prepared using the same method for preparing hollow $TiO_2$ except without adding zeolite as the template.

### Preparation of sandwich-like Pd@TiO₂@Au, hollow TiO₂@Au, Pd@TiO₂@Pt and hollow TiO₂@Pt

The sandwich-like $Pd@TiO_2@Au$ was synthesized by photodeposition of the Au NPs on the surfaces of $Pd@TiO_2$. Specifically, the starting gel of sandwich-like $Pd@TiO_2@Au$ was obtained by dispersing $Pd@TiO_2$ into $HAuCl_4$ (0.06%) solution and adjusting the pH to 8 (adjusted by 0.1 M NaOH). After irradiation at 200–1100 nm for 20 minutes, $Au^{3+}$ was converted into Au NPs. In this way, the sandwich-like $Pd@TiO_2@Au$ was obtained. The hollow $TiO_2@Au$ was obtained by replacing $Pd@TiO_2$ with hollow $TiO_2$. The sandwich-like $Pd@TiO_2@Pt$ was synthesized using the same method except for replacing $HAuCl_4$ by $H_2PtCl_6$. The hollow $TiO_2@Pt$ was prepared by replacing $Pd@TiO_2$ with hollow $TiO_2$.

### Synthesis of Pd-im/silicalite-1 (Pd-im/S1) and Pd-im@TiO₂

For comparison, Pd-im/S1 was obtained using the impregnation method.[27] Typically, 0.23 mL of $(NH_4)_2PdCl_4$ solution (0.28 M) was added into 1 g of S1. After stirring for an hour, the mixture was dried overnight at 80 °C. Finally, Pd-im/S1 was obtained by reducing the dried mixture with hydrogen. Then, $Pd-im@TiO_2$ was prepared using the same method for preparing $Pd@TiO_2$ except for replacing Pd@S1 by Pd-im/S1.

### Synthesis of Pd–Au-im@TiO₂ and Pd–Pt-im@TiO₂

$Pd–Au-im@TiO_2$ and $Pd–Pt-im@TiO_2$ were prepared using the impregnation approach. The metal loadings in $Pd–Au-im@TiO_2$ and $Pd–Pt-im@TiO_2$ were controlled to be comparable with those of sandwich-like $Pd@TiO_2@Au$ and $Pd@TiO_2@Pt$ accordingly. First, Pd@S1 was impregnated with $HAuCl_4$ and $H_2PtCl_6$ solutions, respectively. Then, $Pd–Au-im@S1$ and $Pd–Pt-im@S1$ were obtained by reducing the above two mixtures with hydrogen at 400 °C for 2 h. Finally, $Pd–Au-im@TiO_2$ and $Pd–Pt-im@TiO_2$ were obtained by growing $TiO_2$ on the outside surface of $Pd–Au-im@S1$ and $Pd–Pt-im@S1$, respectively, followed by etching the zeolite with NaOH solution. The methods for the growth of $TiO_2$ and the etching details are the same as those for the preparation of sandwich-like $Pd@TiO_2@Au$.

### Material characterization

Powder X-ray diffraction was performed on a Rigaku Smart Lab X-ray diffractometer using Cu Kα radiation ($\lambda = 1.5418$ Å) in the $2\theta$ range from 4° to 80°. Scanning electron microscopy (SEM)

**1672** | *Mater. Chem. Front.*, 2020, **4**, 1671–1678

This journal is © The Royal Society of Chemistry and the Chinese Chemical Society 2020

images and energy dispersive X-ray (EDX) spectrometry images were obtained using a JSM-7800F (Japan) electron microscope. The transmission electron microscopy (TEM) images and EDX spectrometry images were obtained using a Tecnai F20 electron microscope. The metal loading was determined using inductively coupled plasma (ICP) analyses on a PerkinElmer Optima 3300 DV ICP instrument. X-ray photoelectron spectroscopy (XPS) was carried out on an ESCALAB 250 spectrometer. UV-vis absorption spectra were obtained using a SHIMADZU UV-2550 spectrophotometer (200–800 nm). The photoluminescence (PL) spectral measurements were conducted on a SHIMADZU RF-5301pc spectrofluorophotometer. The PL lifetime decay curves were plotted using a HORIBA Scientific FluoroMax-4 spectrofluorometer.

## Photocatalytic measurements

Typically, 10 mg of the photocatalyst was dispersed in 20 mL of an aqueous solution containing 4 mL of methanol, then the solution was transferred into a quartz vessel. After being vacuumed for 20 min to remove the dissolved air, the vessel was irradiated by a 300 W Xenon lamp under simulated solar light (200–1100 nm) with a light intensity of 250 mW cm$^{-2}$. The gas products generated from photocatalytic water splitting were analyzed periodically using an Agilent 7890A gas chromatograph (GC) with a thermal conductivity detector (TCD).

## Photocurrent measurements

The electrochemical experiments were performed on a CHI 660E electrochemistry work station in Na$_2$SO$_4$ (0.5 M) solution. Platinum wire and the AgCl/Ag electrode (saturated with KCl) were used as the counter electrode and the reference electrode, respectively. The working electrodes were made by loading the samples on indium-tin oxide (ITO). In detail, 10 mg of the photocatalysts was dispersed in 200 μL of deionized water, and then the obtained slurry was dropped onto ITO to form a square with the area of 1 cm$^2$ followed by drying at 50 °C for 30 min. Following dropping 20 μL of Nafion on the surface of the photocatalysts, the photoelectrodes of hollow TiO$_2$, hollow TiO$_2$@Pt, Pd@TiO$_2$ and Pd@TiO$_2$@Au were obtained. Light illumination was provided by a 300 W Xe lamp with the light intensity of 300 mW cm$^{-2}$.

# Results and discussion

The synthesis process of the sandwich-like hollow-structured Pd@TiO$_2$@Au photocatalyst is shown in Fig. 1. First, ultrasmall Pd NPs were obtained by using an MFI type zeolite (silicalite-1) as the host matrix and [Pd(NH$_2$CH$_2$CH$_2$NH$_2$)$_2$]Cl$_2$ as the metal precursor, respectively, using the method developed by our group.[31] Specifically, the precursor of Pd NPs was introduced to the hydrothermal crystallization process of silicalite-1 (S-1). After calcination and followed by reduction with H$_2$, the ultrasmall Pd NPs confined in silicalite 1 (Pd@S1) were obtained. Subsequently, Pd@S1 was covered with a layer of amorphous TiO$_2$ after mixing Pd@S1 in tetrabutyl titanate (TBOT) and ammonia solution at 45 °C for 24 h. Following calcination at 450 °C for 2 h, Pd@S1@TiO$_2$ with anatase TiO$_2$ was obtained.

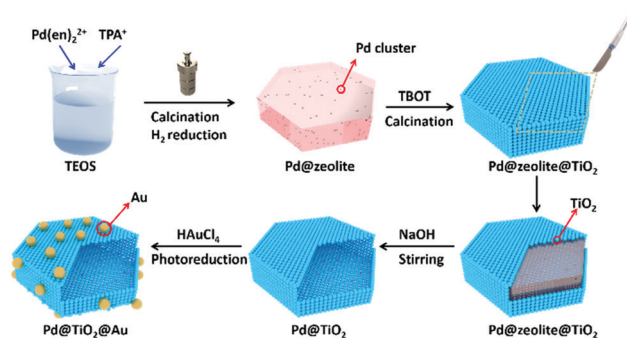

Fig. 1 Schematic illustration for the preparation of the sandwich-like Pd@TiO$_2$@Au photocatalyst.

Afterwards, Pd@S1@TiO$_2$ was transformed into hollow-structured Pd@TiO$_2$ after being treated with the NaOH solution. In this way, the sandwich-like hollow-structured Pd@TiO$_2$@Au was achieved by photo-reducing HAuCl$_4$ on the outer surface of Pd@TiO$_2$. For comparison, hollow TiO$_2$ and conventional TiO$_2$ NPs were also prepared by using pure S1 as the sacrificial substrate and without adding zeolites, respectively. In addition, Pd-im@TiO$_2$ with larger Pd NPs was achieved by growing TiO$_2$ on the outside surface of Pd-im/S1 (obtained using the impregnation method). In order to further elucidate the effect of spatially separated cocatalysts on the sandwich-like hollow structured Pd@TiO$_2$@Au photocatalyst, Pd–Au-im@TiO$_2$ with both the cocatalysts (Pd and Au NPs) decorated on the inner surface of hollow TiO$_2$ was prepared.

As shown in the scanning electron microscopy (SEM) and transmission electron microscopy (TEM) images (Fig. 2 and Fig. S1, S2, ESI†), S1, Pd@S1, Pd@TiO$_2$ and the sandwich-like Pd@TiO$_2$@Au all display the shape of a hexagonal prism with the size of about 200–300 nm. According to the TEM images of Pd@S1 obtained



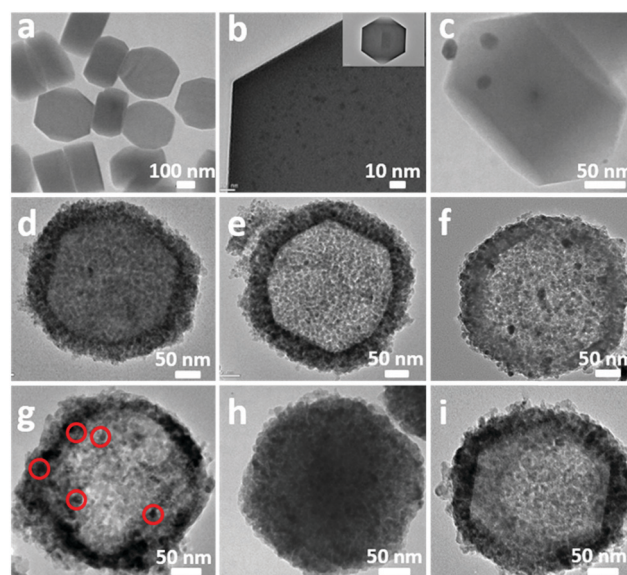Fig. 2 TEM image of Pd@S1 in lower (a) and higher magnification (b); (c) TEM image of Pd-im/S1; (d) TEM image of Pd@S1@TiO$_2$; (e) TEM image of Pd@TiO$_2$; (f) TEM image of Pd@TiO$_2$@Au; (g) TEM image of Pd-im@TiO$_2$; (h) TEM image of S1@TiO$_2$; (i) TEM image of hollow TiO$_2$.

This journal is © The Royal Society of Chemistry and the Chinese Chemical Society 2020

*Mater. Chem. Front.*, 2020, **4**, 1671–1678 | **1673**

by the *in situ* process, the ultrasmall Pd clusters ($<2$ nm) are uniformly located inside the zeolite crystals (Fig. 2a and b). In comparison, the Pd-im/S1 sample prepared by the impregnation method possesses a larger size of Pd NPs ($\sim 10$ nm), as shown in Fig. 2c. The TEM image of Pd@S1@TiO$_2$ in Fig. 2d shows that a layer of TiO$_2$ with the thickness of about 35 nm covers the outer surface of Pd@S1. As shown in Fig. 2e and f, both Pd@TiO$_2$ and Pd@TiO$_2$@Au exhibit a hollow structure. Due to the small size, the inner Pd NPs are invisible. The Au NPs in Pd@TiO$_2$@Au decorated on the outer surface of hollow Pd@TiO$_2$ are about 10 nm in size. In contrast, the Pd NPs in the hollow Pd-im@TiO$_2$ (Fig. 2g) are more obvious for their larger size. In addition, the hexagonal S1@TiO$_2$ (Fig. 2h) and hollow TiO$_2$ (Fig. 2i) and conventional TiO$_2$ NPs (Fig. S3, ESI†) were also obtained.

The SEM and TEM elemental mappings of Pd@TiO$_2$ and Pd@TiO$_2$@Au are shown in Fig. 3a–i and Fig. S4 (ESI†), revealing the existence of Pd, Ti, O and Au elements. The Pd, Ti and O elements are distributed uniformly in hollow-structured Pd@TiO$_2$ and Pd@TiO$_2$@Au. Furthermore, it appears that the Au NPs are deposited on the outside surface of hollow TiO$_2$ in sandwich-like Pd@TiO$_2$@Au (Fig. S4, ESI†). According to the inductively coupled plasma atomic emission spectroscopy (ICP-AES) analysis, the Au and Pd loading in the sandwich-like hollow-structured Pd@TiO$_2$@Au is 4.89 and 0.62 wt%, respectively.

The as-prepared sandwich-like hollow-structured Pd@TiO$_2$@Au photocatalyst was further characterized using X-ray diffraction (XRD). The as-synthesized S1 and Pd@S1 exhibit the typical diffraction peaks of the MFI zeolite structure (Fig. S5, ESI†).[22] For Pd@S1@TiO$_2$, the diffraction peaks belonging to anatase-TiO$_2$ can be obviously seen (Fig. S6, ESI†).[29] According to Fig. S6, S7 (ESI†) and Fig. 4a, all the TiO$_2$-containing samples (TiO$_2$ NPs, hollow TiO$_2$, Pd@TiO$_2$, hollow TiO$_2$@Au and Pd@TiO$_2$@Au) show typical diffraction peaks of anatase-TiO$_2$. Besides, the peaks of face-centered-cubic Au can be seen in the XRD profiles of hollow TiO$_2$@Au and Pd@TiO$_2$@Au.[29]

The UV-vis spectra in Fig. 4b indicate that the existence of both Pd NPs and Au NPs can enhance the light absorption of hollow TiO$_2$. Furthermore, Pd@TiO$_2$@Au with spatially separated Pd NPs and Au NPs exhibits much higher light absorption efficiency than the hollow TiO$_2$ and monometal cocatalyst decorated ones (Pd@TiO$_2$ and hollow TiO$_2$@Au). Besides, TiO$_2$@Au and Pd@TiO$_2$@Au with decorated Au NPs show much higher light

absorption ability in the visible light range, which may be caused by the elevated light absorption due to the SPR effect and the light scattering of Au NPs.[27]

The X-ray photoelectron spectroscopy (XPS) analyses of sandwich-like Pd@TiO$_2$@Au are shown in Fig. 4c–f. There are two peaks belonging to Ti 2p that appear at around 458.8 and 464.7 eV, indicating the Ti$^{4+}$ valence state in octahedral coordination with oxygen.[32] The signal of O 1s exhibits a peak at 530.2 eV corresponding to the Ti–O bonds in the TiO$_2$ lattice, and the peak located at the shoulder (532.4 eV) is related to the oxygen in the surface hydroxyl groups.[33] The peak at 335.1 attributed to Pd 3d$_{5/2}$ is observed in Pd@TiO$_2$@Au, which is related to the zero-valent Pd NPs.[31] The Au 4f spectrum displays two peaks at 83.3 and 87.0 eV with the splitting of 3.7 eV, indicating the metallic nature of Au.[34]

The photocatalytic H$_2$ evolution activities of sandwich-like Pd@TiO$_2$@Au together with hollow TiO$_2$, Pd@TiO$_2$, and hollow TiO$_2$@Au were investigated under simulated solar light. In the photocatalytic reaction system, methanol (CH$_3$OH) was added as the sacrificial agent to react with the holes. As shown in Fig. 5a–b and Fig. S8 (ESI†), all of the hollow-structured photo-catalysts exhibit enhanced hydrogen generation compared to the TiO$_2$ NPs. The H$_2$ evolution rate of hollow TiO$_2$ (14.3 µmol h$^{-1}$) is about 2 times faster than that of the TiO$_2$ NPs (6.5 µmol h$^{-1}$ in Fig. S8, ESI†). This phenomenon can be attributed to the elevated light harvesting induced by the hollow structure. Notably, Pd@TiO$_2$@Au with spatially separated bimetallic cocatalysts shows greatly improved photocatalytic properties. The H$_2$ generation rate of Pd@TiO$_2$ and TiO$_2$@Au reaches up to 210.8 and 119.5 µmol h$^{-1}$, respectively. Significantly, Pd@TiO$_2$@Au gives a H$_2$ generation rate up to 272.3 µmol h$^{-1}$. For comparison, we also prepared sandwich-like Pd@TiO$_2$@Pt by using Pt to replace Au to further test whether different separated bimetallic cocatalysts on TiO$_2$ could still work (Fig. 5c). The morphologies of Pd@TiO$_2$@Pt, hollow TiO$_2$@Pt and Pt-im/Pd@S1 are shown in Fig. S9 and S10 (ESI†). As expected, Pd@TiO$_2$@Pt with similar types of spatially separated cocatalysts (Pd NPs and Pt NPs) shows an enhanced hydrogen evolution rate (648.6 µmol h$^{-1}$) compared to TiO$_2$ NPs and hollow TiO$_2$. In addition, Pd@TiO$_2$@Pt gives a higher elevated hydrogen evolution rate than Pd@TiO$_2$ (210.8 µmol h$^{-1}$) and TiO$_2$@Pt (464.0 µmol h$^{-1}$). To further
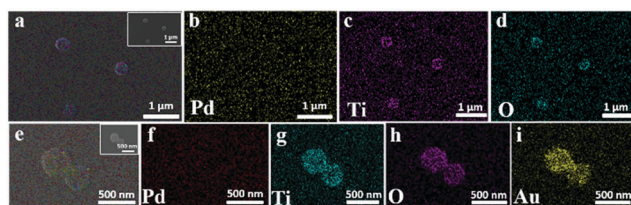


**Fig. 3** Elemental mapping images of Pd@TiO$_2$ (a)–(d) and sandwich-like Pd@TiO$_2$@Au (e)–(i): (a and e) the corresponding overlapped elemental mapping images of Pd, Ti, and O and Pd, Ti, O and Au respectively, and the insets in (a) and (e) are the corresponding SEM images; (b and f) Pd mapping images; (c and g) Ti mapping images; (d and h) O mapping images; and (i) Au mapping image.
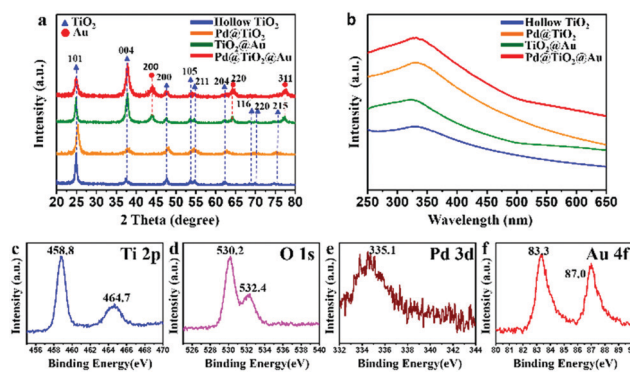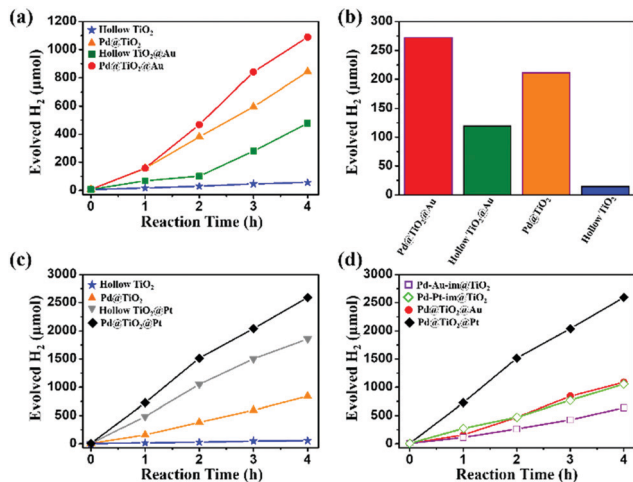


**Fig. 4** (a) XRD profiles and UV-vis spectra (b) of hollow TiO$_2$, Pd@TiO$_2$, hollow TiO$_2$@Au and sandwich-like Pd@TiO$_2$@Au; (c)–(f) XPS spectra of sandwich-like Pd@TiO$_2$@Au.

Fig. 5 (a) $H_2$ generation over the sandwich-like Pd@TiO$_2$@Au catalyst, hollow TiO$_2$, Pd@TiO$_2$ and hollow TiO$_2$@Au; (b) $H_2$ evolution rates based on the corresponding catalysts in Fig. 5a; (c) $H_2$ generation over the Pd@TiO$_2$@Pt catalyst and the corresponding controls; (d) $H_2$ generation over Pd–Au-im@TiO$_2$ and Pd–Pt-im@TiO$_2$ for comparison with Pd@TiO$_2$@Au and Pd@TiO$_2$@Pt.



Fig. 6 Photocurrent generation performance (a), PL spectra (b), PL lifetime decay curves (c) and the bar chart of PL decay time (d) of hollow TiO$_2$, Pd@TiO$_2$, hollow TiO$_2$@Au and sandwich-like Pd@TiO$_2$@Au.

demonstrate the effects of the spatially separated cocatalysts on TiO$_2$, Pd–Au-im@TiO$_2$ and Pd–Pt-im@TiO$_2$ with both bi-noble metal NPs decorated within the hollow cavity were also prepared to compare with Pd@TiO$_2$@Au and Pd@TiO$_2$@Pt correspondingly (Fig. 5d). The $H_2$ generation rates of Pd–Au-im@TiO$_2$ and Pd–Pt-im@TiO$_2$ are 159.3 and 264.2 μmol h$^{-1}$, respectively, which are much lower than that of Pd@TiO$_2$@Au and Pd@TiO$_2$@Pt decorated with the spatially separated bimetallic cocatalyst. Therefore, we can conclude that spatially separated bi-noble metals play an important role in enhancing the photocatalytic efficiency.

On the other hand, the size effect of Pd NPs plays an important role in the photocatalytic efficiency of Pd@TiO$_2$. For comparison, Pd-im@TiO$_2$ with larger sized Pd NPs was also obtained by replacing Pd@S1 with Pd-im/S1 to work as the sacrificial substrate. As shown in Fig. S11 (ESI†), Pd-im@TiO$_2$ shows a lower hydrogen evolution rate (163.5 μmol h$^{-1}$) than Pd@TiO$_2$ (210.8 μmol h$^{-1}$). Therefore, the smaller sized Pd NPs synthesized by *in situ* crystallization of the zeolite can further improve the catalytic properties of TiO$_2$. It is worth mentioning that the hydrogen generation rate of sandwich-like Pd@TiO$_2$@Au (272.3 μmol h$^{-1}$) with the quantum efficiency of 1.64% (Fig. S12, ESI†) is superior to most of the TiO$_2$-based photocatalysts for photocatalytic hydrogen generation under similar conditions (Table S1, ESI†).[34–42]

Fig. 6a shows the photocurrent generation performance of hollow TiO$_2$, Pd@TiO$_2$, hollow TiO$_2$@Au and sandwich-like Pd@TiO$_2$@Au. It can be clearly seen that the existence of Pd NPs and Au NPs can improve the photocurrent density. Specifically, the sandwich-like Pd@TiO$_2$@Au with spatially separated cocatalysts exhibits the highest photocurrent density, demonstrating the efficient photoinduced charge separation properties. To further investigate the charge separation properties of the as-prepared
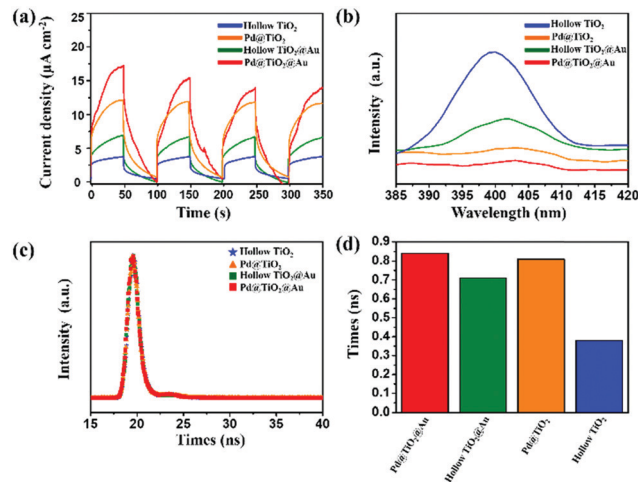
photocatalysts, the photoluminescence (PL) emission spectrum was recorded. As shown in Fig. 6b, all the samples exhibit characteristic peaks at around 400 nm. In detail, all the TiO$_2$ hybrids with decorated cocatalysts (Pd NPs or Au NPs) show weaker PL emission compared to hollow TiO$_2$, which may be attributed to the lower Fermi level of Pd NPs and Au NPs.[21] Furthermore, the PL emission of Pd@TiO$_2$ is lower than that of hollow TiO$_2$@Au, suggesting that Pd@TiO$_2$ possesses greater charge transfer ability than hollow TiO$_2$@Au. Notably, the sandwich-like Pd@TiO$_2$@Au exhibits the weakest PL emission among all of the samples, further confirming the superior charge separation performance. To better understand the behaviour of the photo-excited charge carriers, the time-resolved fluorescence decay spectra of the as-prepared photocatalysts were also studied (Fig. 6c). According to the bar chart of PL decay time shown in Fig. 6d, the sandwich-like Pd@TiO$_2$@Au displays a longer decay time than the other samples, further indicating the superior charge separation of the photocatalyst with spatially separated bimetals.

The proposed mechanism of photocatalytic hydrogen generation over the sandwich-like Pd@TiO$_2$@Au catalyst is shown in Fig. 7. Upon irradiation by incident light, holes are generated
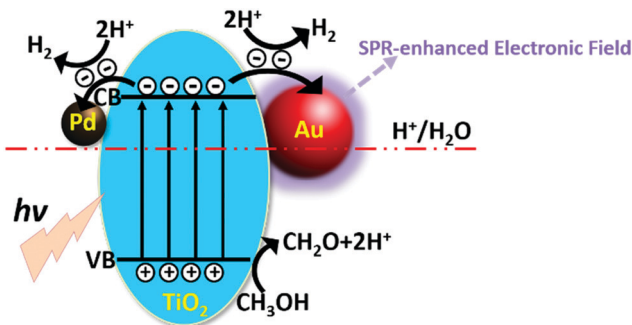


Fig. 7 Proposed mechanism of photocatalytic hydrogen generation over the Pd@TiO$_2$@Au catalyst.

on the valence band (VB) of $TiO_2$ and photo-induced electrons are produced on the conduction band (CB). Subsequently, the photo-induced electrons can be quickly transferred from $TiO_2$ to the cocatalysts (Pd NPs and Au NPs).[43,44] In addition, the SPR effect induced by the Au NPs on the outside surface of $TiO_2$ can stimulate an enhanced electronic field, which can not only improve the generation rate of electron–hole pairs, but also facilitate the charge transfer.[45] Meanwhile, charge separation can be further improved by the ultrasmall size effect of Pd NPs located on the inner surface of $TiO_2$.[46] In this way, more efficient charge transfer and quantum efficiency can be obtained. Moreover, the photo-generated holes on the VB of $TiO_2$ can be used to oxidize the scavenger ($CH_3OH$) to produce $H^+$ ions. Afterward, the $H^+$ ions can combine with the electrons on the CB of $TiO_2$ or cocatalysts to produce $H_2$. Specifically, the spatially separated bimetallic cocatalysts can further enhance the photocatalytic properties of sandwich-like Pd@$TiO_2$@Au due to the enhanced charge separation, as shown in Fig. 6.

## Conclusions

A hollow-structured $TiO_2$ decorated with spatially separated bimetallic cocatalysts (Pd@$TiO_2$@Au) was obtained by using a zeolite as the sacrificial substrate. Pd@$TiO_2$@Au exhibits superior photocatalytic hydrogen generation ability based on the factors below: first, the hollow structure of $TiO_2$ can not only enhance light utilizing ability by repeated light reflection and refraction, but also provide more active reaction sites and facilitate mass transfer through the enhanced specific surface area. Second, the spatially separated bimetallic cocatalysts (Pd and Au) can further increase the photocatalytic charge transfer and separation by fully utilizing the photo-induced charges on both the inner and outer surfaces of the excited $TiO_2$. Thirdly, the SPR effect induced by the Au NPs on the outside surface of $TiO_2$ can stimulate an enhanced electronic field, which can not only improve the generation rate of electron–hole pairs, but also facilitate the charge transfer. Fourth, the ultra-small Pd NPs synthesized by the *in situ* crystallization process of zeolite can further elevate the charge separation efficiency. The facile approach demonstrated here holds great promise for the design of highly efficient photocatalysts for the application of environmental purification and solar-to-hydrogen energy conversion.

## Conflicts of interest

There are no conflicts to declare.

## Acknowledgements

## Notes and references

1 J. L. Wu, Z. Y. Zhang, B. K. Liu, Y. R. Fang, L. Wang and B. Dong, UV-Vis-NIR-driven plasmonic photocatalysts with dual-resonance modes for synergistically enhancing $H_2$ generation, *Sol. RRL*, 2018, **2**, 1800039.

2 Y. Liu, Z. Y. Zhang, Y. R. Fang, B. K. Liu, J. D. Huang, F. J. Miao, Y. A. Bao and B. Dong, IR-driven strong plasmonic-coupling on Ag nanorices/$W_{18}O_{49}$ nanowires heterostructures for photo/thermal synergistic enhancement of $H_2$ evolution from ammonia borane, *Appl. Catal., B*, 2019, **252**, 164–173.

3 D. P. Dong, C. X. Yan, J. D. Huang, N. Lu, P. Y. Wu, J. Wang and Z. Y. Zhang, An electron-donating strategy to guide the construction of MOF photocatalysts toward co-catalyst-free highly efficient photocatalytic $H_2$ evolution, *J. Mater. Chem. A*, 2019, **7**, 24180–24185.

4 M. Y. Zhang, Y. Qi and Z. Y. Zhang, AgBr/BiOBr nano-heterostructure-decorated polyacrylonitrile nanofibers: a recyclable high-performance photocatalyst for dye degradation under vsible-light irradiation, *Polymers*, 2019, **11**, 1718.

5 P. Zhang, D. Y. Wan, Z. Y. Zhang, G. D. Wang, J. H. Hu and G. S. Shao, RGO-functionalized polymer nanofibrous membrane with exceptional surface activity and ultra-low airflow resistance for PM2.5 filtration, *Environ. Sci.: Nano*, 2018, **5**, 1813–1820.

6 Q. M. Sun, N. Wang, J. H. Yu and J. C. Yu, A hollow porous CdS photocatalyst, *Adv. Mater.*, 2018, **30**, 1804368.

7 Y. G. Zhu, Z. Y. Zhang, N. Lu, R. N. Hua and B. Dong, Prolonging charge-separation states by doping lanthanide-ions into {001}/{101} facets-coexposed $TiO_2$ nanosheets for enhancing pho-cmssmark tocatalytic $H_2$ evolution, *Chin. J. Catal.*, 2019, **40**, 413–423.

8 C. Tang, L. F. Liu, Y. L. Li and Z. F. Bian, Aerosol spray assisted assembly of $TiO_2$ mesocrystals into hierarchical hollow microspheres with enhanced photocatalytic performance, *Appl. Catal., B*, 2017, **201**, 41–47.

9 M. Z. Ge, Q. S. Li, C. Y. Cao, J. Y. Huang, S. H. Li, S. N. Zhang, Z. Chen, K. Q. Zhang, S. S. Al-Deyab and Y. K. Lai, One-dimensional $TiO_2$ nanotube photocatalysts for solar water splitting, *Adv. Sci.*, 2017, **4**, 1600152.

10 Y. X. Zhao, Y. F. Zhao, R. Shi, B. Wang, G. I. N. Waterhouse, L. Z. Wu, C. H. Tung and T. R. Zhang, Tuning oxygen vacancies in ultrathin $TiO_2$ nanosheets to boost photocatalytic nitrogen fixation up to 700 nm, *Adv. Mater.*, 2019, **31**, 1806482.

11 Z. W. Seh, S. H. Liu, M. Low, S. Y. Zhang, Z. L. Liu, A. Mlayah and M. Y. Han, Janus Au–$TiO_2$ photocatalysts with strong localization of plasmonic near-fields for efficient visible-light hydrogen generation, *Adv. Mater.*, 2012, **24**, 2310–2314.

12 Z. Q. Liang, Y. C. Guo, Y. J. Xue, H. Z. Cui and J. Tian, 1T-phase $MoS_2$ quantum dots as a superior co-catalyst to Pt decorated on carbon nitride nanorods for photocatalytic hydrogen evolution from water, *Mater. Chem. Front.*, 2019, **3**, 2032–2040.

**1676** | *Mater. Chem. Front.*, 2020, **4**, 1671–1678

This journal is © The Royal Society of Chemistry and the Chinese Chemical Society 2020

13  J. L. He, S. Li, D. Lyu, D. F. Zhang, X. Wu and Q. H. Xu, Aggregation induced emission enhancement by plasmon coupling of noble metal nanoparticles, *Mater. Chem. Front.*, 2019, **3**, 2421–2427.

14  L. Cheng, D. N. Zhang, Y. L. Liao, F. Li, H. W. Zhang and Q. J. Xiang, Constructing functionalized plasmonic gold/titanium dioxide nanosheets with small gold nanoparticles for efficient photocatalytic hydrogen evolution, *J. Colloid Interface Sci.*, 2019, **555**, 94–103.

15  S. Q. Kong, X. M. Song, C. W. Zhang, W. Wang and G. C. Yan, Photocatalytic activity and photodegradation rate constant of Au–TiO$_2$ nanofilms by magnetron sputtering, *Rare Met. Mater. Eng.*, 2018, **47**, 3316–3320.

16  Z. Y. Zhang, S. W. Cao, Y. S. Liao and C. Xue, Selective photocatalytic decomposition of formic acid over AuPd nanoparticle-decorated TiO$_2$ nanofibers toward high-yield hydrogen production, *Appl. Catal., B*, 2015, **162**, 204–209.

17  Z. Y. Zhang, A. R. Li, S. W. Cao, M. Bosman, S. Z. Li and C. Xue, Direct evidence of plasmon enhancement on photocatalytic hydrogen generation over Au/Pt-decorated TiO$_2$ nanofibers, *Nanoscale*, 2014, **6**, 5217–5222.

18  H. B. Yu, X. H. Wang, H. W. Sun and M. X. Huo, Photocatalytic degradation of malathion in aqueous solution using an Au–Pd–TiO$_2$ nanotube film, *J. Hazard. Mater.*, 2010, **184**, 753–758.

19  Y. Shiraishi, H. Sakamoto, Y. Sugano, S. Ichikawa and T. Hirai, Pt-Cu bimetallic alloy nanoparticles supported on anatase TiO$_2$: highly active catalysts for aerobic oxidation driven by visible light, *ACS Nano*, 2013, **7**, 9287–9297.

20  A. Gallo, M. Marelli, R. Psaro, V. Gombac, T. Montini, P. Fornasiero, R. Pievo and V. Dal Santo, Bimetallic Au–Pt/TiO$_2$ photocatalysts active under UV-A and simulated sunlight for H$_2$ production from ethanol, *Green Chem.*, 2012, **14**, 330–333.

21  K. Qian, B. C. Sweeny, A. C. Johnston-Peck, W. X. Niu, J. O. Graham, J. S. DuChene, J. J. Qiu, Y. C. Wang, M. H. Engelhard, D. Su, E. A. Stach and W. D. Wei, Surface plasmon-driven water reduction: gold nanoparticle size matters, *J. Am. Chem. Soc.*, 2014, **136**, 9842–9845.

22  T. L. Cui, W. Y. Ke, W. B. Zhang, H. H. Wang, X. H. Li and J. S. Chen, Encapsulating palladium nanoparticles inside mesoporous MFI zeolite nanocrystals for shape-selective catalysis, *Angew. Chem., Int. Ed.*, 2016, **55**, 9178–9182.

23  L. C. Liu, U. Diaz, R. Arenal, G. Agostini, P. Concepcion and A. Corma, Generation of subnanometric platinum with high stability during transformation of a 2D zeolite into 3D, *Nat. Mater.*, 2017, **16**, 1272.

24  S. Goel, S. I. Zones and E. Iglesia, Encapsulation of metal clusters within MFI via interzeolite transformations and direct hydrothermal syntheses and catalytic consequences of their confinement, *J. Am. Chem. Soc.*, 2014, **136**, 15280–15290.

25  H. J. Cho, D. Kim, J. Li, D. Su and B. J. Xu, Zeolite-encapsulated Pt nanoparticles for tandem catalysis, *J. Am. Chem. Soc.*, 2018, **140**, 13514–13520.

26  W. Li, Y. H. Deng, Z. X. Wu, X. F. Qian, J. P. Yang, Y. Wang, D. Gu, F. Zhang, B. Tu and D. Y. Zhao, Hydrothermal etching assisted crystallization: A facile route to functional yolk-shell titanate microspheres with ultrathin nanosheets-assembled double shells, *J. Am. Chem. Soc.*, 2011, **133**, 15830–15833.

27  J. Du, J. Qi, D. Wang and Z. Y. Tang, Facile synthesis of Au@TiO$_2$ core-shell hollow spheres for dye-sensitized solar cells with remarkably improved efficiency, *Energy Environ. Sci.*, 2012, **5**, 6914–6918.

28  N. Zhang, S. Q. Liu, X. Z. Fu and Y. J. Xu, Synthesis of M@TiO$_2$ (M = Au, Pd, Pt) core-shell nanocomposites with tunable photoreactivity, *J. Phys. Chem. C*, 2011, **115**, 9136–9145.

29  W. G. Tu, Y. Zhou, H. J. Li, P. Li and Z. G. Zou, Au@TiO$_2$ yolk-shell hollow spheres for plasmon-induced photocatalytic reduction of CO$_2$ to solar fuel via a local electromagnetic field, *Nanoscale*, 2015, **7**, 14232–14236.

30  P. Zhang and X. W. Lou, Design of heterostructured hollow photocatalysts for solar-to-chemical energy conversion, *Adv. Mater.*, 2019, **31**, 1900281.

31  N. Wang, Q. M. Sun, R. S. Bai, X. Li, G. Q. Guo and J. H. Yu, In situ confinement of ultrasmall Pd clusters within nanosized silicalite-1 zeolite for highly efficient catalysis of hydrogen generation, *J. Am. Chem. Soc.*, 2016, **138**, 7484–7487.

32  J. B. Cai, X. Q. Wu, S. X. Li, F. Y. Zheng, L. C. Zhu and Z. H. Lai, Synergistic effect of double-shelled and sandwiched TiO$_2$@Au@C hollow spheres with enhanced visible-light-driven photocatalytic activity, *ACS Appl. Mater. Interfaces*, 2015, **7**, 3764–3772.

33  Z. F. Jiang, W. Wei, D. J. Mao, C. Chen, Y. F. Shi, X. M. Lv and J. M. Xie, Silver-loaded nitrogen-doped yolk-shell mesoporous TiO$_2$ hollow microspheres with enhanced visible light photocatalytic activity, *Nanoscale*, 2015, **7**, 784–797.

34  M. G. Wang, J. Han, H. X. Xiong and R. Guo, Yolk@shell nanoarchitecture of Au@rGO/TiO$_2$ hybrids as powerful visible light photocatalysts, *Langmuir*, 2015, **31**, 6220–6228.

35  B. Cao, G. S. Li and H. X. Li, Hollow spherical RuO$_2$@TiO$_2$@Pt bifunctional photocatalyst for coupled H$_2$ production and pollutant degradation, *Appl. Catal., B*, 2016, **194**, 42–49.

36  Q. R. He, H. Sun, Y. X. Shang, Y. N. Tang, P. She, S. Zeng, K. L. Xu, G. L. Lu, S. Liang, S. Y. Yin and Z. N. Liu, Au@TiO$_2$ yolk-shell nanostructures for enhanced performance in both photoelectric and photocatalytic solar conversion, *Appl. Surf. Sci.*, 2018, **441**, 458–465.

37  K. E. deKrafft, C. Wang and W. B. Lin, Metal–organic framework templated synthesis of Fe$_2$O$_3$/TiO$_2$ nanocomposite for hydrogen production, *Adv. Mater.*, 2012, **24**, 2014–2018.

38  J. K. Zhang, Z. B. Yu, Z. Gao, H. B. Ge, S. C. Zhao, C. Q. Chen, S. Chen, X. L. Tong, M. H. Wang, Z. F. Zheng and Y. Qin, Porous TiO$_2$ nanotubes with spatially separated platinum and CoO$_x$ cocatalysts produced by atomic layer deposition for photocatalytic hydrogen production, *Angew. Chem., Int. Ed.*, 2017, **56**, 816–820.

39  L. J. Gao, Y. G. Li, J. B. Ren, S. F. Wang, R. N. Wang, G. S. Fu and Y. Hu, Passivation of defect states in anatase TiO$_2$ hollow spheres with Mg doping: realizing efficient photocatalytic overall water splitting, *Appl. Catal., B*, 2017, **202**, 127–133.

40 J. Q. Yan, H. Wu, H. Chen, Y. X. Zhang, F. X. Zhang and S. F. Liu, Fabrication of $TiO_2/C_3N_4$ heterostructure for enhanced photocatalytic Z-scheme overall water splitting, *Appl. Catal., B*, 2016, **191**, 130–137.

41 X. Yu, J. Zhang, Z. H. Zhao, W. B. Guo, J. C. Qiu, X. N. Mou, A. X. Li, J. P. Claverie and H. Liu, NiO–$TiO_2$ p–n heterostructured nanocables bridged by zero-bandgap rGO for highly efficient photocatalytic water splitting, *Nano Energy*, 2015, **16**, 207–217.

42 P. F. Wang, S. H. Zhan, Y. G. Xia, S. L. Ma, Q. X. Zhou and Y. Li, The fundamental role and mechanism of reduced graphene oxide in rGO/Pt–$TiO_2$ nanocomposite for high-performance photocatalytic water splitting, *Appl. Catal., B*, 2017, **207**, 335–346.

43 K. F. Wu, H. M. Zhu, Z. Liu, W. Rodriguez-Cordoba and T. Q. Lian, Ultrafast charge separation and long-lived charge separated state in photocatalytic CdS–Pt nanorod heterostructures, *J. Am. Chem. Soc.*, 2012, **134**, 10337–10340.

44 K. F. Wu, H. M. Zhu and T. Q. Lian, Ultrafast exciton dynamics and light-driven $H_2$ evolution in colloidal semiconductor nanorods and Pt-tipped nanorods, *Acc. Chem. Res.*, 2015, **48**, 851–859.

45 J. B. Lee, S. Choi, J. Kim and Y. S. Nam, Plasmonically-assisted nanoarchitectures for solar water splitting: obstacles and breakthroughs, *Nano Today*, 2017, **16**, 61–81.

46 V. Subramanian, E. E. Wolf and P. V. Kamat, Catalysis with $TiO_2$/gold nanocomposites. effect of metal particle size on the Fermi level equilibration, *J. Am. Chem. Soc.*, 2004, **126**, 4943–4950.